Title	Transducin activates cGMP phosphodiesterase by trapping inhibitory subunit freed spontaneously from the catalytic subunits in solution
Author(s)	淺野, 禎三
Citation	大阪大学, 2019, 博士論文
Version Type	VoR
URL	https://doi.org/10.18910/72622
rights	
Note	

Doctor Thesis

Transducin activates cGMP phosphodiesterase by trapping inhibitory subunit freed spontaneously from the catalytic subunits in solution

（トランスデューシンは水溶液中で触媒サブユニットから自発的に解離した抑制性サブユニットを捕捉することでcGMPホスホジエステラーゼを活性化する）

Sensory Transduction Group
Nanobiology Laboratories
Graduate School of Frontier Biosciences
Osaka University

Teizo Asano

淺野　禎三

March 2019

日本語要旨

　脊椎動物の視細胞では、酵素カスケードは光応答発生メカニズムにおいて重要な役割を果たしている。光を受容し活性化された視物質は、三量体 G タンパク質の一種であるトランスデューシンのαサブユニット（Tα）に結合している GDP の GTP への置換を触媒することにより Tαを活性化する（Tα*）。Tα*はさらに cGMP ホスホジエステラーゼ（PDE）を活性化する。PDE は 2 種類の触媒サブユニット（PDEα、PDEβ）および 2 つの抑制性サブユニット（PDEγ）からなる四量体タンパク質である。PDEαと PDEβはアミノ酸配列の70%以上が一致している相同性の高いサブユニットであり、それぞれが cGMP を GMP へと加水分解する活性部位を持っている。PDEγはそれぞれの触媒サブユニットに結合することで cGMP 分解活性を抑制している。Tα*は PDEγと結合することで触媒サブユニットの活性部位にかかっていた抑制を解除することにより PDE 活性化する。PDE の活性化によって細胞内の cGMP 濃度の低下が起こり視細胞膜上にある cGMP 依存性陽イオンチャネルが閉じることで、過分極性の光応答が生じる。

　Tα*による PDE の活性化反応は、触媒サブユニットに結合した状態の PDEγに Tα*が結合し、PDEγを触媒サブユニットの活性化部位から解離させることにより起こると信じられている。しかしながら近年の PDEγ·PDEα複合体および PDEγ·Tα*複合体の構造解析研究により、PDEγは C 末端領域にあるアミノ酸（Asp-63 から Ile-87）で Tα*と結合しており、また PDEαとも同様に C 末端領域にあるアミノ酸（Leu-60 から Ile-87）で結合していることが明らかになった。PDEγはほぼ同じ領域のアミノ酸によって PDEαまたは Tα*と結合しているという事実は、PDEγは PDEαおよび Tα*とは同時には結合することはできないことを意味しており、従来信じられている活性化メカニズムでは Tα*による PDE の活性化を十分に説明できないことを示唆している。そこで私は Tα*による PDE の活性化メカニズムを明らかにしたいと考えた。

　まず PDEγと各タンパク質との相互作用解析を行った。高純度に精製したタンパク質を用いて Tα*と PDEγまたは四量体 PDE との相互作用を表面プラズモン共鳴法により測定した結果、PDEγは四量体 PDE と比べてより高いアフィニティで Tα*と結合することが明らかになった。この結果は、Tα*は触媒サブユニットと結合した状態の PDEγとは複合体を形成しにくい可能性を示している。つまり Tα*による PDE の活性化は、従来考えられているような触媒サブユニットに結合した状態の PDEγに Tα*が結合することで PDEγを触媒サブユニットの活性化部位から解離させるというメカニズムではなく、触媒サブユニットから解離した PDEγを Tα*が結合し PDEγの触媒サブユニットへの再結合を阻害することで、PDE の活性化状態を維持している可能性が考えられた（トラッピングメカニズム）。そこでこのメカニズムによる活性化の反応式を解き、得られた理論式と実験結果が一致するかどうかを調べることにした。そのために PDEγ·PDEα複合体および PDEγ·Tα*複合体の解離定数（K_D）を実験的に求めた。

まず PDEγ と触媒サブユニットとの K_D を pH assay 法を用いて水溶系、膜系でそれぞれ測定した。その結果、水溶系における K_D は 10pM、一方で膜系における K_D は 54pM であった。さらに PDEγ と $T\alpha^*$ との K_D を表面プラズモン共鳴法を用いて測定したところ、0.73〜5.6nM という結果が得られた。これらの K_D を理論式に代入し $T\alpha^*$ による PDE の活性化効率を理論的に求め、実験的に求めた値と比較した。その結果、水溶系においてはトラッピングメカニズムは従来のメカニズムよりも、より適切に実験結果を説明することができた。一方で膜系においては、10μM の視物質を含む膜濃度では適切に説明できるが、1.5μM、20μM の視物質を含む膜濃度においては説明できなかった。これはタンパク質の構造が膜環境に影響されるためだと考えられる。

　以上の結果から、$T\alpha^*$ による PDE の活性化は少なくとも水溶系において、トラッピングメカニズムに従って起こっていることが示唆された。

ABSTRACT

Activation of cGMP phosphodiesterase (PDE) by activated transducin α subunit (Tα*) is a necessary step to generate a light response in vertebrate photoreceptors. PDE in rods is a heterotetramer composed of two catalytic subunits, PDEα and PDEβ, and two inhibitory PDEγ subunits, each binding to PDEα or PDEβ, and is activated by relief of the inhibitory constraint of PDEγ on the catalytic subunit. In this activation mechanism, it is widely believed that Tα* binds to PDEγ still bound to the catalytic subunit, and removes or displaces PDEγ from the catalytic subunit. However, recent structural analysis showed that the binding of Tα* to PDEγ still bound to PDEα or PDEβ seems to be unlikely because the binding site of PDEγ to the catalytic subunit overlaps with the binding site to Tα*. To understand the mechanism of activation of PDE by Tα*, I examined the bindings of PDEγ and PDE (PDE$\alpha\gamma\beta\gamma$) to Tα* with surface plasmon resonance and biochemical measurements. My initial study showed a much more effective binding of Tα* to PDEγ than to PDE, and this result suggested an intriguing possibility that Tα* binds to PDEγ freed spontaneously from the catalytic subunit. To test this possibility, I first determined the dissociation constant of the complex of PDEγ and the catalytic subunit (K_{D1}) to estimate the concentration of freed PDEγ, and then that of the complex of PDEγ and Tα* (K_{D2}) to quantify this complex. With these values, one can numerically estimate the PDE activity at a given concentration of Tα*. My estimation reasonably agreed with the result of my biochemical measurement of PDE activation caused by addition of known amounts of Tα* in solution. In the present study, I propose a novel activation mechanism of PDE , the trapping mechanism, in rods in which Tα* activates PDE by trapping PDEγ freed spontaneously from PDE to inhibit its re-binding to the catalytic subunit.

CONTENTS

ABBREBIATIONS

ROS, rod outer segment

Tα*, activated transdusin α subunit

Tα-S*, GTPγS-bound form of Tα*

PDE, cGMP phosphodiesterase

PDEγ (Pγ), inhibitory subunit of PDE

PDEcat (Pcat), catalytic subunit of PDE

K_{D1}, dissociation constant of PDEγ·PDEcat complex

K_{D2}, dissociation constant of PDEγ·Tα* complex

INTRODUCTION

Vertebrates have two types of photoreceptors, rods and cones, in retina. Both rods and cones are consisted of outer segment and inner segment. Photoreceptor cells are responsible for generation for a light response in the outer segment (1, 2). For this, the outer segment contains molecular machinery to convert light signals into electrical signals called phototransduction cascade (Fig. 1). Briefly, after absorption of light, light-activated visual pigment catalyzes the exchange of GDP for GTP on the α subunit of transducin (Tα) to produce a GTP-bound active form of transducin (Tα*). Tα* then activates cGMP phosphodiesterase (PDE). PDE is a heterotetrameric protein composed of two catalytic subunits of similar amino acid sequence (PDEα and PDEβ showing >70 % sequence identity) and two inhibitory subunits (PDEγ) and therefore is in the form of PDE$\alpha\beta\gamma$. Each catalytic subunit has an active site to hydrolyze cGMP to GMP. In the inactive form of PDE, one molecule of PDEγ binds to each of the active sites (PDE$\alpha\gamma$ and PDE$\beta\gamma$), and inhibits hydrolysis of cGMP. (In the followings, I generally use the term of PDE to indicate the inactive form of PDE, PDE$\alpha\beta\gamma$). Tα* binds to inhibitory PDEγ, and relieves its constraint on the active site in the catalytic subunit to activate PDE. This activation of PDE causes hydrolysis of cGMP, leads to closure of cGMP-gated cation channels situated in the plasma membrane of the outer segment, and hyperpolarizes the cell.

In rod cells, this activation mechanism has been well studied. At the step of activation of rhodopsin (visual pigment of rod), a series of structural changes is known. Photon absorption by 11-*cys*-retinal leads an isomerization of 11-*cys*-retinal to all-*trans* retinal. This isomerization triggers the formation of a series of intermediates of rhodopsin in the order of bathorhodopsin, lumirhodopsin, metarhodopsin I and metarhodopsin II (active form of rhodopsin) within a few millisecond. Moreover, activation of Tα by rhodopsin and hydrolysis of cGMP by PDE are described quantitatively. One molecule of activated rhodopsin activates ~100 molecules of

7

transducin per second (3) and one molecule of activated PDE hydrolyzes ~2000 molecules of cGMP per second (4). However, the activation mechanism of PDE by Tα* is not well known.

In the activation process of PDE by Tα*, it is widely believed that Tα* directly binds to PDEγ still bound to the catalytic subunit, and removes or displaces PDEγ from the active site of a catalytic subunit (5, 6). However, this mechanism seems to be unlikely based on the recent structural studies on a PDEγ·PDEα complex and a PDEγ·Tα* complex: most of the amino acid residues in the C-terminal region of PDEγ, from Asp-63 to Ile-87, are in contact with Tα* (7), and almost the same region, from Leu-60 to Ile-87 in PDEγ, is in contact with the catalytic site of PDEα or PDEβ (8). These observations suggest that PDEγ utilizes the same region to bind to Tα* and to the catalytic site of PDEα or PDEβ, and that Tα* and the catalytic subunit cannot bind to this region simultaneously.

To understand the PDE activation mechanism by Tα*, the dissociation constant (K_D) of the PDEγ·Tα* has been measured using biochemical (9), spectroscopic (10) and surface plasmon resonance (SPR) methods (11, 12). In these studies respectively, the K_D of the complex has been reported to be 100 nM, < 0.1 nM and 33-37 nM, which are all low enough to form a complex (13). However, excess amount of Tα* has been reported to be needed to activate PDE (6, 14). In fact, Wensel and Stryer reported the necessity of >2 μM of Tα* to activate a half of 0.6 nM PDE (6). If Tα* binds to PDE with the same K_D as that of the PDEγ·Tα* complex (0.1 − 100 nM, see above), my calculation shows that the concentration of Tα* necessary to activate a half of 0.6 nM PDE should be 0.1 − 100 nM. Thus, the K_D values reported and the concentration of Tα* required for PDE activation do not seem to be consistent, which is probably because of insufficient understandings of activation mechanism of PDE. The activation mechanism of PDE by Tα* is the last poorly understood reaction in phototransduction cascade.

In this study, therefore, I examined the interaction between Tα* and PDEγ, and that

between Tα* and PDE by SPR and biochemical measurements. Based on the kinetic and biochemical measurements together with numerical considerations, I propose a novel activation mechanism of PDE: Tα* activates PDE by trapping PDEγ freed spontaneously from PDE to inhibit its re-binding to the catalytic subunit. I named this novel mechanism as trapping mechanism. The equation derived from trapping mechanism can properly explain the experimental results of PDE activation by Tα*. Moreover, the trapping mechanism would be the mechanism that is required to activate PDE under the restriction of minimizing the dark continuous background noise in rods. By this study, details of all reactions in phototransduction cascade are revealed.
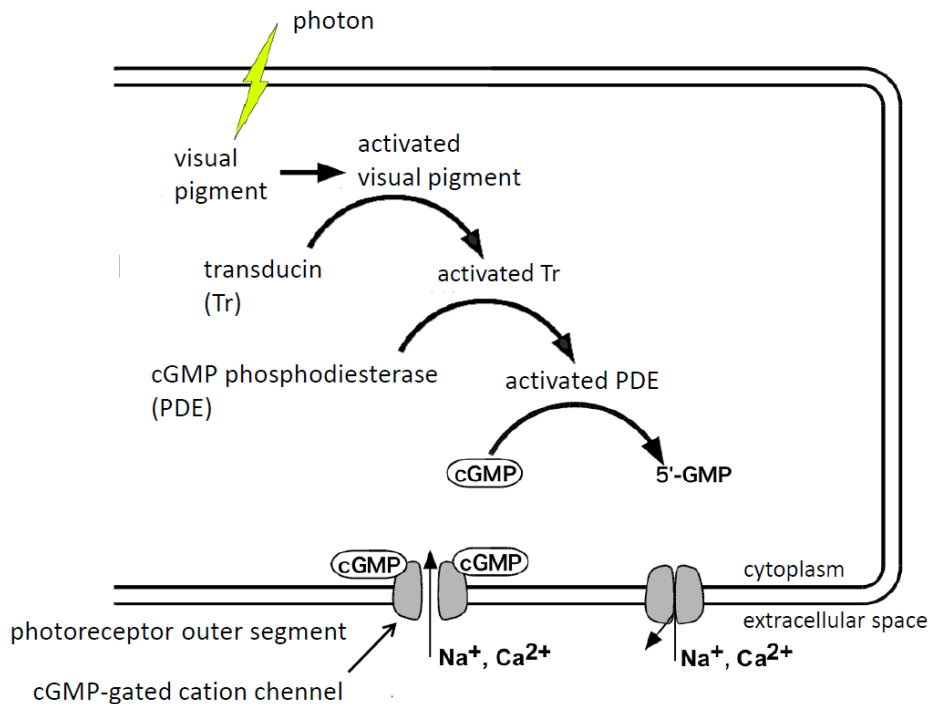

Fig. 1 Phototransduction cascade in photoreceptor cell. These reactions occur in the outer segment of photoreceptor cell. Light signals are converted into electrical signals through this cascade. The mechanisms of each reaction are well studied, however, only PDE activation mechanism by Tα* is not clear yet.

RESULTS

Purification of PDE and Tα-S* from frog retina

To examine the interaction between Tα* and PDE, firstly, I purified each protein from frog retina. Briefly, ROSs dissected form dark-adapted frogs were brushed off the isolated retina. ROS membranes were purified by using a stepwise sucrose gradient formed by two layers of 29 % (w/v) and 36 % (w/v) sucrose in K-gluc buffer. ROS membranes were sedimented at the interface between the two sucrose layers. From the purified ROS membranes, I purified crude PDE and crude GTPγS-bound form of Tα* (Tα-S*). Briefly, purified ROS membranes were homogenized and illuminated in K-gluc buffer. Illuminate ROS membranes were suspended in hypotonic buffer (buffer A) and PDE was extracted into buffer A (Fig. 2a). ROS membranes were resuspended in hypotonic buffer containing GTPγS (buffer B) and Tα-S* plus Tβγ (crude Tα-S*) were extracted into buffer B (Fig. 2a).

To purify PDE, crude PDE was loaded on an anion exchange column and eluted with NaCl gradient. PDE was eluted at 0.47 − 1 M NaCl (Fig. 2b). Purified PDE was loaded on a gel filtration column to exchange the buffer to K-gluc buffer. Purified PDE was subjected to SDS-PAGE and the gels were stained with Oriole Fluorescent Gel Stain Kit to assess the purity of PDE (Fig. 2c). It cannot be detected any protein except for PDE, and therefore I concluded the purity of PDE was almost 100%. Furthermore, I quantified the ratio of gamma to alpha/beta subunits of purified PDE using SDS-PAGE, and found that the ratio is 1.001 ± 0.012 (mean $\pm$ SD, n=3). This indicates that the purified PDE retained enough gamma subunits, and was suitable for my analysis.

Tα-S* was purified from crude Tα-S* using Blue Sepharose and DEAE Sepharose tandem-column. Tβγ was bound to the Blue Sepharose column and most of Tα-S* passed through this column and bound to the DEAE Sepharose column. Tα-S* bound to the DEAE

10

Sepharose column was eluted using NaCl gradient. Tα-S* eluted at 0.7 – 1 M NaCl was collected (Fig. 2d). Purified Tα-S* was loaded on a gel filtration column to exchange the buffer. Purity of purified Tα-S* was assessed with SDS-PAGE and the purity of PDE was almost 100% (Fig. 2e).
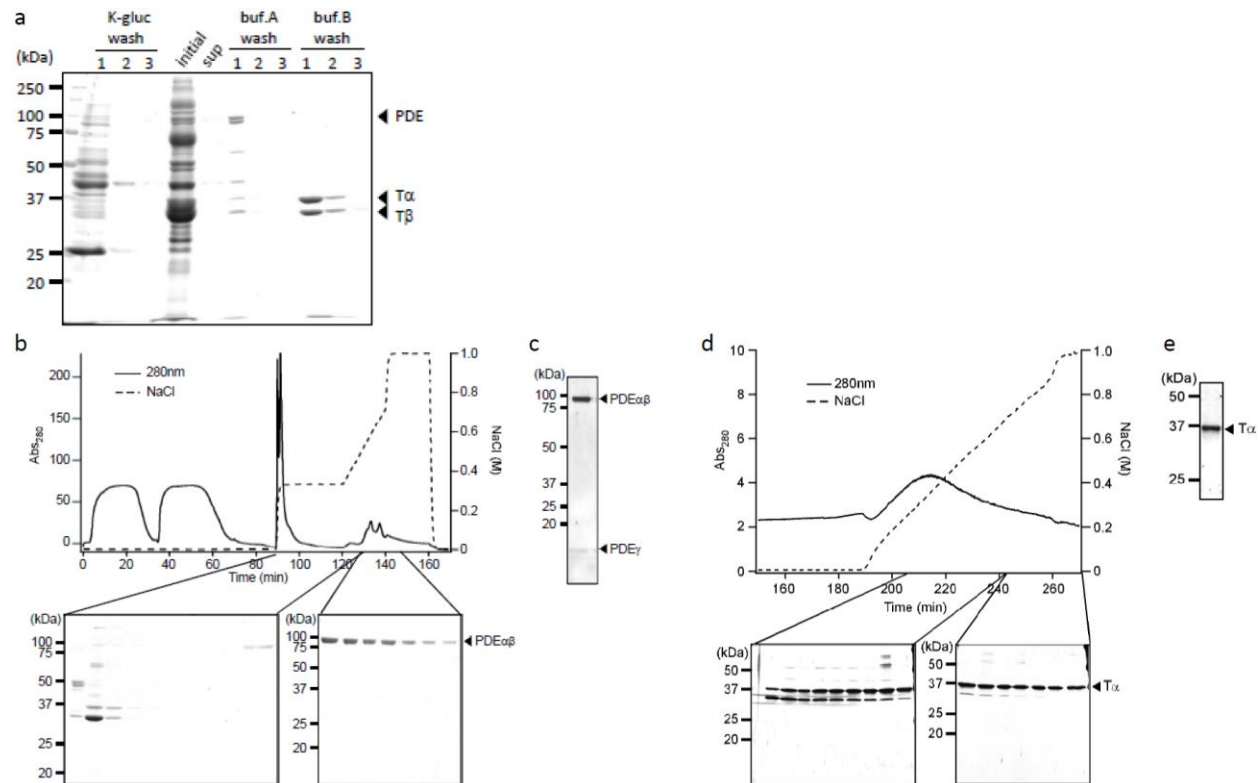

Fig. 2. Purification of PDE and Tα-S*. (a) Extraction of PDE and Tα-S* from ROS membrane. ROS membranes were washed with K-gluc buffer (K-gluc wash). Washed ROS membranes were then suspended in buffer A (buf.A wash) followed by in buffer B (buf.B wash). (b) Purification of PDE using anion exchange column. Crude PDE extracted in buffer A was loaded on a MonoQ column and eluted with NaCl gradient. Protein elution was monitored with UV (upper panel) and eluted fractions were subjected to SDS-PAGE and the gels were stained with Oriole Fluorescent Gel Stain Kit (lower panel). (c) Assessment of the purity of purified PDE. Purified PDE was subjected to SDS-PAGE and the gels were stained with Oriole Fluorescent Gel Stain Kit using bovine serum albumin as a molar standard. (d) Purification of Tα-S* using anion exchange column. Crude Tα-S* extracted in buffer B was loaded on a Blue Sepharose and a DEAE Sepharose tandem-column. After washing, these columns were separated and Tα-S* was eluted from a DEAE Sepharose with NaCl gradient. Protein elution was monitored with UV (upper panel) and eluted fractions were subjected to SDS-PAGE and the gels were stained with Oriole Fluorescent Gel Stain Kit (lower panel). (e) Assessment of the purity of purified Tα-S*. Purity of purified Tα-S*was assessed as described above.

Purification of recombinant PDEγ

To examine the interaction between Tα* and PDEγ, I expressed and purified PDEγ. PDEγ was expressed in E. coli and the cells expressing PDEγ was collected and sonicated. The supernatant containing PDEγ was loaded on a CM Sepharose and the bound proteins were eluted using NaCl gradient (Fig. 3a). Additional purification of PDEγ was carried out using a C18 reverse-phase column with an acetonitrile gradient (Fig. 3b). Purified PDEγ was lyophilized to remove acetonitrile and dissolved in K-gluc buffer. I confirmed that purified PDEγ can inhibit the cGMP hydrolysis activity of trypsin-treated PDE.

Much more effective binding of Tα-S to free PDEγ than to PDEγ still bound to PDE catalytic subunit*

To make sure that Tα* binds much more effectively to free PDEγ than to PDEγ still bound to PDE catalytic subunit, I measured the binding of free PDEγ and that of purified PDE to Tα*
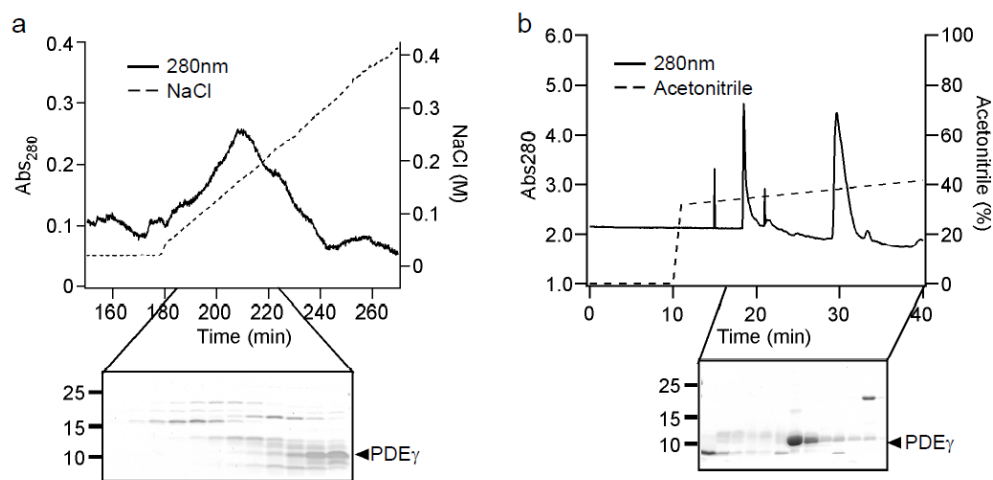

Fig. 3. Purification of PDEγ. (a) Expressed PDEγ was loaded on a CM Sepharose Fast Flow column and eluted with NaCl gradient. Protein elution was monitored with UV (upper panel) and eluted fractions were subjected to SDS-PAGE and the gels were stained with CBB (lower panel). (b) Fractions containing PDEγ were loaded on a C18 reverse-phase column and eluted with acetonitrile gradient. Protein elution was monitored with UV (upper panel) and eluted fractions were subjected to SDS-PAGE and the gels were stained with CBB (lower panel).

with the Surface Plasmon Resonance (SPR) method. For this, I used the guanosine 5'-O-(γ-thio) triphosphate (GTPγS)-bound form of Tα (Tα-S*), an active form of Tα, and immobilized it on the surface of an SPR sensor chip as the common binding target of free PDEγ and PDEγ still bound to PDE catalytic subunit. Fig. 4 shows a series of biding-dissociation time courses of PDEγ and that of PDE (i.e., PDEγ and PDE catalytic subunit complex), both at 1 − 16 nM (horizontal bars). Note that these measurements were made on the same sensor chip, so that it can be compared the binding signals directly at each concentration of PDEγ and PDE. As is seen very clearly, binding of PDEγ was much more effective than that of PDE. It should be mentioned here that the SPR signal is proportional to the mass bound to the immobilized protein. The molecular mass of PDEγ is 9.5 kDa and that of PDE is 216.4 kDa. When the same number of PDE molecules binds to the sensor chip as that of PDEγ, PDE signal should be 23 times (216.4/9.5) larger than the PDEγ signal. The result in Fig. 4, therefore, showed that PDEγ binds to Tα-S* much more effectively than PDE, and raised an intriguing possibility that Tα-S* binds to PDEγ freed spontaneously from PDE (freed PDEγ), not PDEγ in PDE in the activation of PDE.
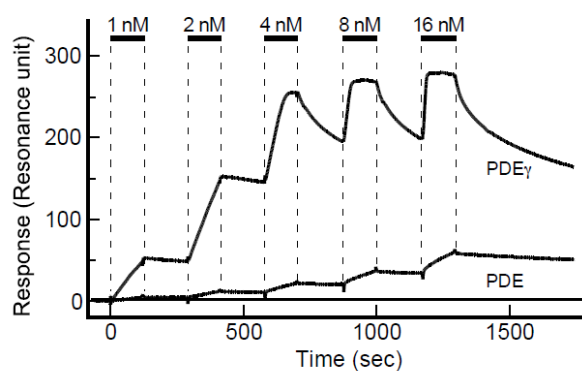

Fig. 4. Comparison of the bindings of PDEγ and PDE to immobilized Tα-S* with the SPR method. PDEγ or PDE was injected at the concentrations indicated. Injections were made as indicated (horizontal bars), and bound proteins were washed out after each injection. Immobilization level of Tα-S* was ~2300 resonance unit (RU).

13

I measured the binding signals using a running buffer that did not contain cGMP throughout the SPR method. It is well known that PDE catalytic subunit has one or two non-catalytic cGMP binding sites (15). When these non-catalytic sites are empty, which is most likely with my purified PDE, Tα* physically removes PDEγ from PDE catalytic subunit upon activation (10). Thus, on injection of PDE, PDE catalytic subunit is removed from PDEγ that is associated with immobilized Tα-S* on the sensor chip. Then, I could expect that the binding signal of PDE is almost the same as that of recombinant PDEγ of the same concentration, which is not the case in Fig. 4. The binding signal of PDE in Fig. 4, therefore, suggests that Tα-S* traps limited amount of PDEγ freed reversibly from PDE.

This consideration led me to determine first the K_D of a complex of PDEγ and the catalytic subunit to estimate the concentration of freed PDEγ. In this estimation, I assumed that the K_D values of the complexes of PDEαγ and PDEβγ are the same, and that the binding and dissociation of PDEγ to and from one catalytic subunit (PDEα, for example) takes place independently on the other catalytic subunit (PDEβ). Because I assumed that PDEα and PDEβ behave indistinguishably, I call either of the catalytic subunits PDEcat in the following.

Determination of the K_D of the complex of PDEγ and PDEcat

To determine the K_D of the complex of PDEγ and PDEcat (PDEγ·PDEcat complex), first I measured the PDE activity using purified PDE at diluted low concentrations in the light without addition of GTP (Fig. 5a, filled circles). As dilution increases, the concentration of freed PDEγ, and therefore, relative PDE activity increases depending on the K_D. The relation between the concentration of PDE and the measured relative PDE activity was fitted with an equation (Equation 5 in Materials and Methods) to determine the K_D of the PDEγ·PDEcat complex (K_{D1}).

The best-fitted K_{D1} of the PDEγ·PDEcat complex in purified PDE was 10 pM (solid curve

14

in Fig. 5a), However, the data points scattered slightly in Fig. 5a so that I could only determine the range of K_{D1}: it was approximately 5-20 pM (broken curves for K_{D1} of 5 and 20 pM) and close to the reported value of <10 pM obtained with purified bovine PDE previously (6). Similar dilution study was made using ROS membranes (filled circles in Fig. 5b). The best-fitted K_{D1} of the PDEγ·PDEcat complex in ROS membranes was 54 pM, and the range was 40 − 60 pM (broken curves for K_{D1} of 40 and 60 pM). It should be mentioned here that freed PDEγ is completely freed from PDEcat. If freed PDEγ is removed from the active site but is still attached to the PDEcat, dilution will not induce the increase in the relative PDE activity because dilution does not affect re-binding of PDEγ to the catalytic subunit. In fact, repeated washes of rod outer segment (ROS) membranes increased relative PDE dark activity (Fig. 6).

*Determination of K_D of the complex of PDEγ and Tα-S**

To measure the K_D of the PDEγ·Tα-S* complex (K_{D2}), I measured it in two configurations using the SPR method (Fig. 7). One configuration was similar to that shown in Fig. 4: Tα-S* was immobilized. In Fig. 7a, 2 − 16 nM PDEγ was perfused until the signal reached to a steady level and bound PDEγ was washed out almost completely at each PDEγ concentration. All of the measured time courses were then globally fitted with a program provided by the manufacturer (black broken traces in Fig. 7a, see Materials and Methods) to determine K_{D2} of the PDEγ·Tα-S* complex. In a total of three different measurements using two different sensor chips, I obtained K_{D2} of 0.73 ± 0.13 nM (mean ± SE, n = 3) for the PDEγ·Tα-S* complex.

The value of K_{D2} was determined in the reversed configuration: PDEγ was immobilized and Tα-S* was perfused (Fig. 7b). In this case, Tα-S* of increasing concentration was perfused before bound Tα-S* was washed out completely (pink trace). Measured time course was fitted with a 1:1 binding with MTL program provided by the manufacturer (black broken trace in Fig.
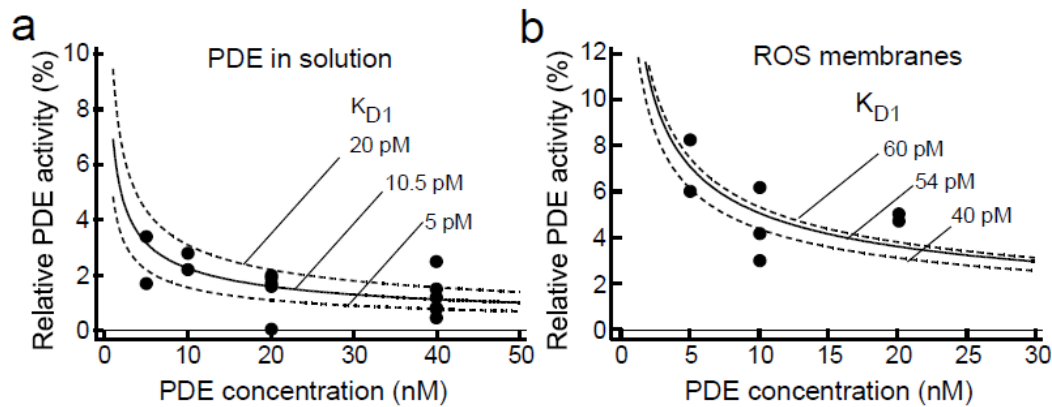
Fig. 5. Determination of K_{D1} of the PDEγ·PDEcat complex. PDE activity was measured using purified PDE (**a**) and ROS membranes (**b**) at the concentrations of PDE shown in the horizontal axis. Each data point shows the result of a single activity measurement. (**a**) The concentration of purified PDE was calibrated with SDS-PAGE. The relation between relative PDE activity and the concentration of PDE was fitted with Equation 5 to determine K_{D1} of the PDEγ·PDEcat complex. The best-fitted K_{D1} in solutions of purified PDE was 10 pM (solid black curve), and the expected curve for K_{D1} of 5 pM and that of 20 pM are also shown (broken curves). (**b**) Similar as in **a**, but PDE content in a ROS membrane suspension was estimated by assuming that the molar ratio of PDE to rhodopsin is 1/270 in ROS membranes (13). The best-fitted K_{D1} was 54 pM (solid curve). Expected curve for K_{D1} of 40 pM and that of 60 pM are also shown (broken curves).
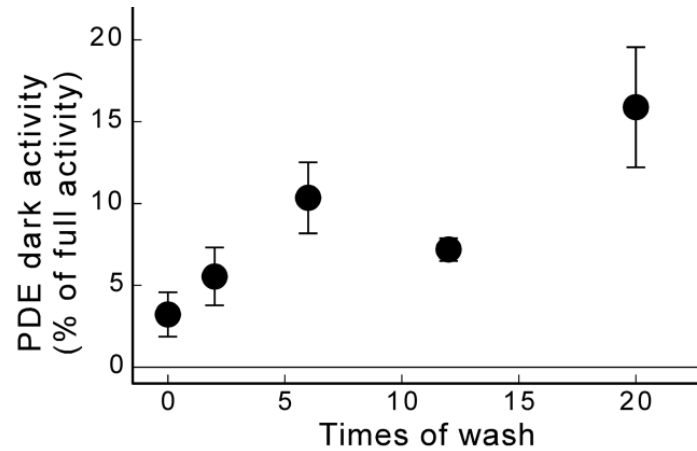

Fig. 6. PDE dark activity increase with extensive washes. ROS membranes were disrupted by passing through a #27 gauge needle for 10 times and freeze-thawed. They were washed at indicated times by centrifugation (150,000 × g, 5 min) with 0.8 × K-gluc buffer, and finally resuspended in K-gluc buffer. PDE dark activity was measured with the pH assay method. The activity is expressed as the % of the full activity measured after treatment with trypsin. The results are indicated as mean ± SD (n = 5-9 except for the point at 6 washes where n = 2 and the result at this point is indicated as mean ± the range of variation).

16

7b, see Materials and Methods). From the fitting results, K_{D2} was estimated to be 5.6 ± 1.3 nM (mean $\pm$ SE, n = 5). (According to the manufacturer's protocol, the same dissociation constant can be obtained no matter whether bound protein is completely washed out as in Fig. 7a or not as in Fig. 7b). Obtained values of K_{D2} in two configurations (Tα-S* immobilized or PDEγ immobilized) were ~8 times different (0.73 nM/ 5.6 nM = 1/7.7). Although immobilizations of Tα-S* and PDEγ were designed not to affect the binding site seriously (see Materials and Methods), immobilization seemed to affect K_{D2} slightly. I, therefore, concluded that K_{D2} is $0.73 -$ 5.6 nM, which is consistent with the values of $0.1 - 33$ nM reported previously utilizing various methods for the measurement (6, 8-10).
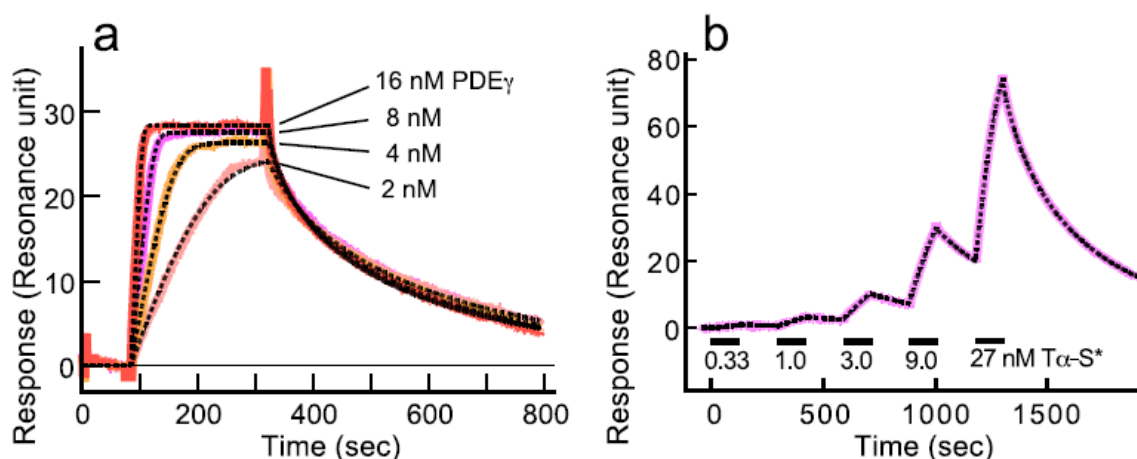

Fig. 7. Determination of K_{D2} of the PDEγ·Tα-S* complex. (**a**) SPR measurements of the binding of PDEγ to immobilized Tα-S*. PDEγ was injected at various concentrations indicated, and perfused until the binding signal was almost saturated. The bound proteins were washed out almost completely after each of the injections. Immobilization level of Tα-S* was ~400 RU. The binding signals (solid traces) were fitted globally using a Heterogeneous Ligand with MTL program to calculate K_{D2}, and it was 0.73 ± 0.13 nM (mean $\pm$ SE, n = 3). Flow rate was 10 μl/min. (**b**) SPR measurements of the binding of Tα-S* to immobilized PDEγ. Tα*-S was injected at indicated concentrations and perfused for 125 sec (horizontal bars) for the binding and then washed out for 175 sec each time. The binding signal (pink solid trace) was globally fitted using a 1:1 binding with MTL program (black broken trace) to calculate K_{D2}. The best-fitted K_{D2} was 5.6 ± 1.3 nM (mean $\pm$ SE, n = 5). Immobilization level of PDEγ was ~100 RU. Flow rate was 30 μl/min.

Validation of the novel mechanism of PDE activation of purified PDE in solution

So far, I revealed that Tα-S* shows much higher affinity to PDEγ than PDE and that PDEγ freed from PDE could be the target of Tα-S*. This result led me to propose a novel mechanism of PDE activation in vertebrate photoreceptors. In the novel mechanism, PDEγ is freed from PDEcat reversibly according to the K_{D1} of the complex of PDEγ·PDEcat. Tα* then traps freed PDEγ with the K_{D2} of the complex of PDEγ·Tα* to activated PDE.

In Figs. 5 and 7, I determined the range of K_{D1} of the PDEγ·PDEcat complex for purified PDE (Fig. 5a) and PDE in ROS membranes (Fig. 5b), and the range of K_{D2} of the PDEγ·Tα-S* complex (Fig. 7). To validate this novel mechanism, I then examined whether this mechanism can explain the activation of PDE by Tα-S* of known concentrations with use of an equation (Equation 10 in Method) formulated for this mechanism.

Fig. 8a shows the measurement of activation of purified PDE by purified Tα-S* in solution at indicated concentrations with the pH assay method (14, 16). The pH decrease accompanied by
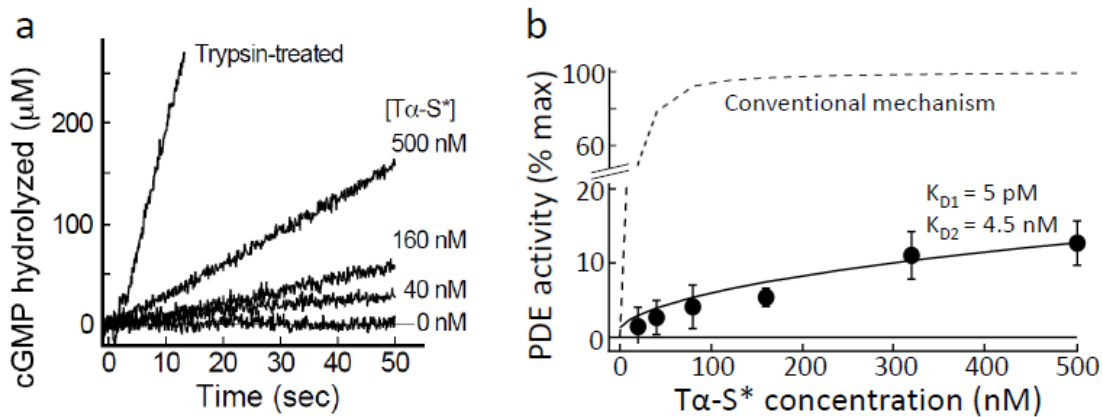

Fig. 8. Activation of purified PDE by purified Tα-S* in a solution. (**a**) Sample traces of PDE activity measurement by the pH assay method in a solution containing ~15 nM PDE and various concentration of Tα-S* indicated. Full PDE activity was determined after treatment with trypsin (trypsin-treated). (**b**) PDE activation as a function of concentration of Tα-S* added. Vertical axis shows the % of full PDE activity. Each data point is a mean ± SE (n = 6 except for the point at 10 nM Tα-S*, where n = 3). The data points were fitted with Equation 10 formulated under the conditions that PDE is activated through the trapping mechanism with K_{D1} = 5 pM and K_{D2} = 4.5 nM (solid curve, see text). Broken curve shows the theoretical curve with the conventional activation mechanism, where K_D = 4.5 nM (see text).

hydrolysis of cGMP was calibrated, and the PDE activity was determined from the slope. Full PDE activity was determined after treatment with trypsin (trypsin-treated). PDE activity at a given GTPγS concentration is expressed as the % of the full PDE activity, and the summarized result is shown in Fig. 8b (filled circles and bars showing mean ± SE). Then, the relation between the relative PDE activity and the Tα-S* concentration was fitted with Equation 10. As shown above, I determined the range of K_{D1} in solution (5 − 20 pM, Fig. 5a) and that of K_{D2} (0.73 − 5.6 nM, Fig. 7), and for this reason, I tried to examine whether I can explain PDE activation by Tα-S* in Fig. 8 with these dissociation constants in those ranges. First, I used K_{D1} of 10 pM, but could not obtain a best-fitted value of K_{D2} within the range of K_{D2} I determined in Fig. 7. For this, I set K_{D1} at 5 pM, for example, and then determined K_{D2} that provides the best fit to the PDE activation curve. The value of K_{D1} was increased by 1 pM step and the best-fitted K_{D2} was determined each time. I then found that at each K_{D1} value from 2 pM to 6 pM, I can find a K_{D2} value that gives a reasonable fit to the PDE activation curve in Fig. 8b. Interestingly, each pair of K_{D1} and K_{D2} I determined showed similar goodness of fit (χ^2, Table 1), and I show the result of K_{D1} = 5 pM and K_{D2} = 4.5 nM in Fig. 8b (solid curve). I tried to estimate the activation curve of PDE by Tα-S* with the conventional binding mechanism (which Tα* binds to PDEγ still bound to PDEcat, and displaces or removes PDEγ from PDEcat to activate PDE) under the condition of K_D = 4.5 nM. The expected curve deviated greatly from the measured result (thick broken curve in Fig. 8b). From this result, I concluded that Tα-S* activates PDE by trapping PDEγ freed reversibly from PDE and by inhibiting its re-binding to PDEcat. An alternative possibility is that Tα-S* binds to PDE (PDEαβ or PDEγ still bound to PDEαβ). However, this possibility can be excluded because the binding of PDE to Tα-S* is weak (Fig. 4). PDE activation with use of purified PDE in solution was measured only at 15 nM PDE. It is because at higher concentrations of purified PDE, the measurement was not possible because of protein

19

aggregation.

Validation of the novel mechanism for activation of PDE in ROS membrane suspension

As shown above, it is highly possible that purified PDE is activated by the novel mechanism. Then, I examined whether this mechanism is applied to PDE in ROS membranes. In the measurement of PDE activity in an illuminated ROS membrane suspension, I added GTPγS at a concentration lower than that of Tα, of which concentration was estimated on the assumption that the molar ratio of Tα to rhodopsin in 1/10 (13). It is to limit the amount of Tα-S* by the amount of added GTPγS (14). In previous study, PDE activation by addition of GTPγS is dependent on the ROS membrane concentration: the lower the concentration, the lower the maximum PDE activation. For this reason, ROS membranes containing rhodopsin of 1.5, 10 and 20 μM (abbreviated as 20 μM rhodopsin membranes, for example) were used to measure the PDE activation at various concentrations of Tα-S*. The activity was measured similarly as in Fig. 8a, and the results are shown in Fig. 9 (circles and bars showing mean $\pm$ SE). Note that the horizontal axis is different in each panel, which is because the maximum Tα-S* concentration should be equal to the concentration of Tα at different membrane concentrations (0.15 μM Tα in 1.5 μM rhodopsin membranes, for example). As reported previously (14), in 20 μM rhodopsin membranes, I obtained almost a full PDE activity that is observed in trypsin-treated ROS membranes (Fig. 9 red circles). Then, I fitted the results in Fig. 9 with Equation 10 to estimate K_{D1} and K_{D2} in ROS membranes at each membrane concentration. As shown in Fig. 5b, I found that the range of K_{D1} in ROS membranes is in the range of 40 – 60 pM. I, therefore, arbitrary set K_{D1} at 40 – 60 pM with 5 pM step, and determined K_{D2} each time. The results are summarized in Table 2. Each pair of K_{D1} and K_{D2} reasonably fits to the PDE activation curve in ROS membranes without significant differences at each ROS membrane concentration (see χ^2 for each

20

membrane concentration in Table 2). Because I obtained the value of 54 pM as K_{D1} in ROS membranes (Fig. 5b), fitting result with K_{D1} of 55 pM is shown at each membrane concentration (Fig. 9).

In Table 2, best-fitted K_{D2} values varied significantly depending on the ROS membrane concentration, and they decreases as membrane concentration increases: at a constant K_{D1} value of 55 pM, the best-fitted K_{D2} are 23.6, 0.201 and 0.0565 nM in 1.5, 10 and 20 μM rhodopsin membranes, respectively. Apparent ROS membrane concentration-dependent changes in K_{D2} suggest the loss of intrinsic Tα-S* from membranes (see Discussion). Although K_{D2} values were not in the K_{D2} range I observed in Fig. 7 (0.73 – 5.6 nM) in 1.5 and 20 μM rhodopsin membranes (23 and 0.0565 nM, respectively), my analysis seemed to explain PDE activation by Tα-S* in ROS membranes the trapping mechanism as well (but, see Discussion). At physiological concentrations of 0.3 mM Tα* and 22.2 μM PDEcat, obtained under the assumption that the rhodopsin concentration is 3 mM and that the transducin and PDE content are 1/10 (13) and 1/270 (4), respectively, of that of rhodopsin, we obtained PDEcat activation of 93 %.
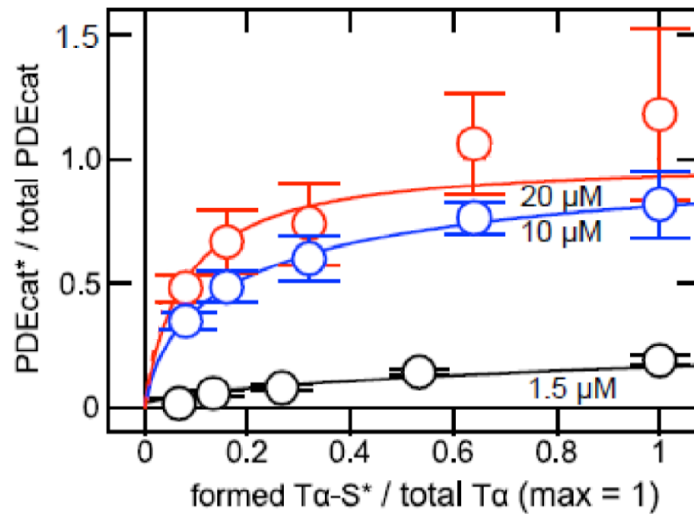

Fig. 9. Activation of PDE with Tα-S* in ROS membrane. Percentage of PDE activation is shown as a function of Tα-S* concentration in suspensions of 1.5 (black circles), 10 (blue ciecles) and 20μM (red circles) rhodopsin membranes. Each data point is a mean ± SE (n = 3-6). The data points were fitted by Equation 10 with fixed K_{D1} (55 pM, see text) and K_{D2} of 23.6 nM (black curve), 0.201 nM (blue curve) and 0.0565 nM (red curve).

DISCUSSION

In the activation mechanism of photoreceptor PDE, it has been generally believed that Tα* binds to PDE, and removes or displaces PDEγ from the active site of PDEcat (conventional mechanism; Fig. 10a). However, my analysis showed that Tα* (actually Tα-S*) binds much more effectively to PDEγ than to PDE (Fig. 4), which is not consistent with the conventional mechanism in Fig. 10a. Furthermore, with the conventional activation mechanism, Tα*-dependent PDE activation could not be explained quantitatively in solution (Fig. 8). These results raised an intriguing possibility that PDEγ freed spontaneously from PDE, not that associated with PDE, is the actual target of Tα* in the activation of PDE. To examine this possibility, I determined the dissociation constant of the PDEγ·PDEcat complex (K_{D1}, 5-20 pM; Fig. 5) and that of the PDEγ·Tα-S* complex (K_{D2}, 0.73-5.6 nM; Fig. 7). Using these dissociation constants, PDE activation is reasonably explained as follows (Fig. 10b). After light stimulation, rhodopsin is activated and many molecules of Tα* are formed. Only a small portion of PDEγ is freed from PDEcat in the dark according to the K_{D1}, which is at least a part of the cause of PDE dark activity. Tα* traps freed PDEγ to form a complex with the K_{D2} to inhibit re-binding of PDEγ to PDEcat, and keeps PDEcat remaining active. Another PDEγ still associated with PDE would be freed from PDEcat with the K_{D1} and the freed PDEγ will be trapped by other Tα* to increase the PDE activity in the light. PDEγ will be released from a PDEγ·Tα* complex when GTP in Tα* is hydrolyzed. Released PDEγ will re-bind to PDEcat with the K_{D1}. This K_{D1} (5-20 pM) is lower about 100 times than that of the PDEγ·Tα-S*complex (0.73-5.6 nM), which would be the reason why the concentration of Tα* required for activation of PDE is much higher than the K_{D2} of the PDEγ·Tα-S*complex. In the following, I call this activation mechanism the trapping mechanism.

According to the equation formulated based on this mechanism (Equation 10), K_{D1} and K_{D2}

in the ranges determined experimentally (Fig. 5a and Fig. 7) gave good fit to the PDE activation curve (Fig. 8 and Table 1) in the case of solution. In the case of membrane suspension, with keeping the K_{D1} in the range determined experimentally in Fig. 5b, K_{D2} was slightly out of the range determined in Fig. 7 (Table 2) (see below). Nonetheless, overall, I believe that PDE activation by Tα* is explained reasonably by the trapping mechanism: Tα* activates PDE by trapping PDEγ freed reversibly from PDEcat with the dissociation constant K_{D1} to inhibit its re-binding to PDEcat.

In the fitting of PDE activation in ROS membrane suspension, best-fitted K_{D2} decreased as the membrane concentration increased: at a constant value of K_{D1} of 55 pM, K_{D2} was 23.6 nM in 1.5 μM rhodopsin membranes, and it decreased significantly to 0.0565 nM in 20 μM rhodopsin membranes (Table 2). Apparently, K_{D2} that can be determined in a ROS membrane suspension is dependent on the membrane concentration. The reason for this is not known. However, it was previously found that ~65 % Tα-S* is eluted from 0.75 μM rhodopsin membranes, but ~50 % from 15 μM rhodopsin membranes in carp (14). This 15 % of Tα-S* remaining in excess in 15 μM rhodopsin membranes could be almost sufficient to activate all of PDEcat molecules, considering the Tα/rhodopsin molar ratio is 1/10 (13) and the PDE/rhodopsin (i.e., 2PDEcat/rhodopsin) molar ratio is 1/270 (4): the molar ratio of 15 % of Tα-S* to PDEcat is ~2:1. It is possible that there could be two types of Tα*. One type binds to membranes tightly and the other loosely. I speculate that the loosely-bound Tα* becomes soluble rather easily at low membrane concentrations, but it remains in the membranes at high membrane concentrations to contribute significantly to activate PDEcat (see below) and to lower apparent K_{D2}. In fact, Tα has been known to be differentially lipidated with 65 % of unsaturated and 30 % of saturated C12 or C14 fatty acids (17).

The trapping mechanism explains PDE activation in solution with K_{D1} and K_{D2}, both

determined experimentally (Fig. 8). It also explains the activation of PDE in ROS membranes (Fig. 9). However, the values of K_{D2} in ROS membranes were not determined experimentally and I am not sure whether those values are correct or not. Tα* and PDE in a disk membrane are undoubtedly situated at certain orientations on the disk membrane in which molecules are densely packed, which probably increases the chance of encounter of Tα* to PDEγ. In this case, Equation 10 cannot be applied directly. Additionally, membrane environment probably influences the conformation of a protein at both inactive and active state. In this case, reaction processes that are not seen in a solution may take place in membranes. Together with the effect of cGMP-binding to the non-catalytic site of PDEcat, further study is necessary to understand the mechanism of PDE activation in membranes. However, because PDEγ binds to PDEcat or Tα* using the same region, Tα* should bind to PDEγ after the dissociation or displacement of PDEγ from PDEcat even when the dissociation or displacement is induced after multistep interaction between Tα* and PDEγ as suggested (18, 19).

My study was made in frog. However, the trapping mechanism seems to be present in other species. In bovine, it has been known that similarly as in frog, excess amount of Tα* is required to activate PDE and that PDE dark activity is increased by dilution of PDE and ROS membranes (6). In frog, it has been known that PDEγ·Tα* complex is found in solution at a nearly physiological ionic concentration (5), which is consistent with the trapping mechanism shown in Fig. 8b. However, in bovine, PDEγ·Tα* complex is found in membranes at a similar ionic concentration (6), and this observation does not seems to be consistent with the trapping mechanism. I believe that this difference in the solubility of PDEγ·Tα* complex would be due to the difference in the solubility of Tα*: it is known that PDEγ·Tα* complex can be extracted at 100 mM Tris-HCl in frog (20) but only at <15 mM Tris-HCl in bovine (21). As in frog, bovine PDEγ is probably freed from PDEcat as inferred from the requirement of high concentrations of

Tα* for PDE activation and also from the increase in the dark activity by dilution of PDE. However, bovine PDEγ·Tα* complex could be present on the membranes because of association of Tα* with membranes at physiological ionic concentrations. Although the biochemical studies show the elution of frog PDEγ·Tα* complex from the membranes, it does not mean that the same situation takes place in living frog rods. Even in truncated frog ROS that is perfused with an external solution continuously, light response recovers to the original dark level even after a light stimulus (22), which could not be explained if all of the PDEγ·Tα* complex are eluted out from a truncated rod. It is possible that Tα* in the PDEγ·Tα* complex is weakly associated with membranes in living frog rods.

In this study, I propose that Tα* traps freed PDEγ to inhibit re-binding to PDEcat and keeps it remaining active. The advantage of this mechanism would be that the only necessary step is to trap PDEγ already freed from PDEcat, which would be effective: if Tα* needs to bind to PDEγ still associated with PDEcat, Tα* may sometimes fail to remove the inhibitory constraint because of low K_D (10 pM) of the PDEγ·PDEcat complex. In case Tα* binds to freed PDEγ, the role of Tα* is just to maintain the active form of PDE, which is more instantaneous in detection of light.

Another possible significance, or rather fundamental requirement of the trapping mechanism, would stem from the characteristics of rod cells. Rods are known as low noise light detectors. Visual pigment, rhodopsin, is very stable (23), so that the reliability of photon detection in rods is very high. It has been also known that continuous background dark noise, which would be caused by PDE dark activity, is very low (24). This low PDE dark activity would probably be due to a stable PDEγ·PDEcat complex, of which K_{D1}. If Tα* needs to remove or displace PDEγ associated tightly with PDEcat, the K_{D2} of a PDEγ·Tα* complex should be at least at an equivalent level to that of a PDEγ·PDEcat complex. In addition, common site in PDEγ

is used for its binding to PDEcat and to Tα* (7, 8). Under these circumstances, the most effective and reliable way to activate PDE would be to trap freed PDEγ. In other words, the trapping mechanism would be the mechanism that is required to activate PDE under the restriction of minimizing the dark continuous background noise in rods.

Overall rod phototransduction system seems to be designed for the same purpose. Content of PDE is low: it is approximately 1/270 of rhodopsin and 1/27 of transducin (4, 13). The concentration of cGMP in the ROS is several μM which is well below the Michaelis constant of PDE, typically 100 μM or so (13). All these seem to contribute to reduce the dark continuous background noise induced by dark PDE activity. Possibly, cones are also low PDE dark noise detectors: high concentrations of Tα* is required to activate cone PDE (14), PDE content is approximately similar to that in rods (14) and the cGMP concentration in a cone outer segment is a few μM (25).

In this study, I tried to reveal the activation mechanism of PDE by Tα* which is the last poorly understood reaction in phototransduction cascade and I proposed the trapping mechanism based on the kinetic and biochemical measurements together with numerical considerations. This mechanism can explain the experimental result of low efficiency of PDE activation by Tα* which has been unexplained phenomenon. Moreover, this mechanism would be the mechanism that is required to activate PDE under the restriction of minimizing the dark continuous background noise in rods. By my study, details of all reactions in phototransduction cascade are revealed.
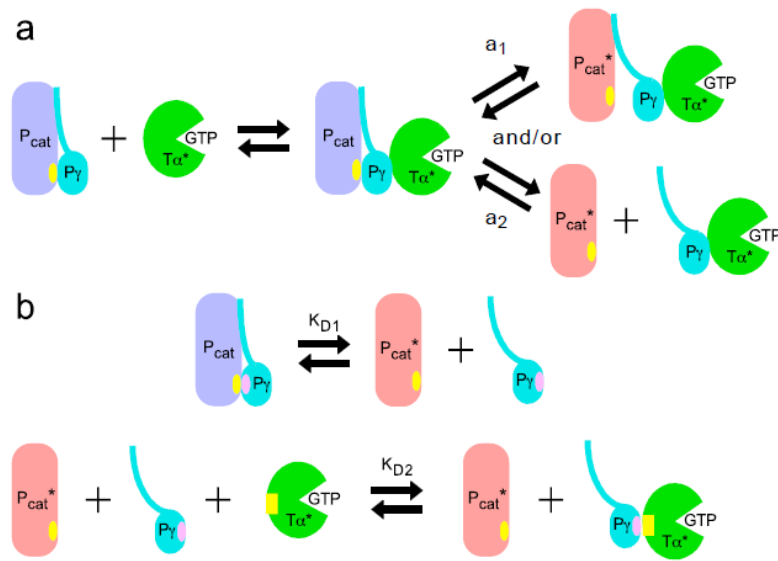
Fig. 10. Possible PDE activation mechanisms. (**a**) Conventional mechanism. In the inactive state of PDE (purple), PDEγ (Pγ) binds to the PDE catalytic subunit (PDEα or β, indicated as Pcat) at the binding site on the catalytic subunit (yellow oval). Activated Tα (Tα*) binds to PDEγ to displace (**a₁**) and/or remove PDEγ (**a₂**) from the catalytic subunit to activate PDE (pale red). (**b**) Trapping mechanism. PDEγ is bound to the catalytic subunit at the binding site of PDEγ (pink oval) and that of the catalytic subunit (yellow oval), but PDEγ is freed reversibly from the catalytic subunit according to the dissociation constant, K_{D1} (**upper**). This freed PDEγ is trapped by Tα* with the dissociation constant, K_{D2}, at the binding site of PDEγ (pink oval) to Tα* (yellow rectangular) to inhibit re-binding of PDEγ to the catalytic subunit (**lower**).

27

Materials and Methods

Preparation of rod outer segment (ROS) membranes from frog

Frogs (*Rana catesbeiana*) were cared according to the institutional guidelines of ethics committee (Permit Number: FBS-15-003). ROS membranes were prepared basically as described previously using a stepwise sucrose density gradient (26). Briefly, frogs were dark-adapted overnight before use. ROSs were brushed off the isolated retinae into a potassium gluconate buffer (K-gluc buffer; 115 mM potassium gluconate, 10 mM HEPES, 2.5 mM KCl, 2 mM $MgCl_2$, 0.2 mM EGTA, 0.1 mM $CaCl_2$, and 1 mM dithiothreitol (DTT), pH 7.5), and isolated ROSs in the buffer were filtrated through a nylon mesh (~95 μm of pore size) to remove fragments of retinal tissues. The pass-through containing probably disrupted ROSs was layered on the top of a stepwise sucrose gradient formed by two layers of 29 % (w/v) and 36 % (w/v) sucrose in K-gluc buffer, and centrifuged at $13,000 \times g$ for 20 min. After the centrifugation, ROS membranes were sedimented at the interface between the two sucrose layers. The membranes were then suspended in K-gluc buffer to reduce the sucrose concentration to <~1/2 of the original value (29 − 36 %), and centrifuged at $20,000 \times g$ for 20 min. The sedimented ROS membranes were then washed twice with K-gluc buffer to remove soluble proteins and sucrose with centrifugation at $20,000 \times g$ for 2 min, frozen in liquid nitrogen and stored at -80 °C until use.

To quantify the yield of the ROS membranes, an aliquot of the membranes was solubilized using 40 mM hexadecyl-trimethyl-ammonium bromide, and the amount of rhodopsin in the membranes was quantified spectrophotometrically with assuming that the molar absorption coefficient of frog rhodopsin is 40,000 $M^{-1}cm^{-1}$ at 500 nm. All of these manipulations were carried out in complete darkness with the aid of an infrared image converter (NVR 2015; NEC, Tokyo, Japan).

Extraction of PDE and GTPγS-bound form of Tα from ROS membranes*

Crude PDE and crude GTPγS-bound form of Tα* were extracted basically as described previously (14, 20). Purified ROS membranes from 30 retinae were homogenized in 2 ml K-gluc buffer and illuminated with >430 nm light for 10 min on ice using a 155 watt halogen lamp at a distance of 10 cm. With this illumination, rhodopsin in ROS membranes was activated and formed a complex with Tα. Then, illuminated ROS membranes were washed with K-gluc buffer, and suspended in a low ionic strength buffer (buffer A: 5 mM HEPES-NaOH, 0.1 mM EDTA, 1 mM DTT, pH7.5). PDE was extracted from ROS membranes into buffer A, and the suspension was centrifuged at $50,000 \times g$ for 15 min to obtain crude PDE in the supernatant.

ROS membranes were then resuspended in a low ionic strength buffer containing GTPγS, a non-hydrolyzable GTP analog (buffer B; 5 mM HEPES-NaOH, 0.5 mM $MgCl_2$, 1 mM DTT, 10 μM GTPγS, pH 7.5), to exchange GDP for GTPγS on Tα complexed with light-activated rhodopsin. Both Tα-S*and Tβγ were dissociated from the membranes and extracted into the buffer. The membranes were centrifuged at $50,000 \times g$ for 15 min, and the supernatant containing extracted Tα-S* plus Tβγ (crude Tα-S*) was collected.

*Purification of PDE and Tα-S**

Crude PDE was loaded on a Mono Q PC 1.6/5 column (ÄKTAmicro system, GE Healthcare) and a 0 - 1 M NaCl gradient in buffer C (10 mM HEPES-NaOH, 2 mM $MgCl_2$, 1 mM DTT, pH7.5) containing 0.005 % (v/v) Tween 20 was applied. Eluted fractions at 0.47 - 1 M NaCl containing purified PDE were concentrated using a Spin-X UF column (M_r 30,000 cutoff, Corning). Purified PDE was then loaded on a Superdex 200 PC 10/300 GL column (ÄKTAmicro system, GE Healthcare) pre-equilibrated with an elution buffer (K-gluc buffer containing 0.005 % (v/v) Tween 20), and eluted at a flow rate of 200 μl/min to change the buffer. Fractions

containing PDE was concentrated using a Spin-X UF column and obtained PDE was stored at -80 °C until use. An aliquot of purified PDE was subjected to SDS-PAGE and the gels were stained with Oriole Fluorescent Gel Stain Kit (Bio-Rad) to assess the purity of PDE and also to quantify its amount using bovine serum albumin as a molar standard. Purity of PDE was almost 100 %.

Tα-S* was purified from crude Tα-S* according to the method reported previously (20). Briefly, a Blue Sepharose 6 Fast Flow column (GE Healthcare) and a DEAE Sepharose Fast Flow column (GE Healthcare) were connected in tandem in this order for the purification. Before loading the proteins, the tandem-column was pre-equilibrated with buffer C. Then, a solution of crude Tα-S* supplemented with 2 mM MgCl$_2$ was loaded on the column. The column was washed with buffer C sufficiently to remove unbound proteins, and then the Blue Sepharose column and the DEAE Sepharose column were separated: frog Tβγ bound to the Blue Sepharose column, and most of Tα-S* passed through this column and bound to the DEAE Sepharose column. Thus, Tα-S* bound to the DEAE Sepharose column was eluted using a 0 - 1 M NaCl gradient in buffer C. Tα-S* was then concentrated using a Spin-X UF column (M_r 10,000 cutoff, Corning). The buffer was changed to K-gluc buffer containing 0.005 % (v/v) Tween 20 using a Superdex 75 PC 3.2/30 column (ÄKTAmicro system, GE Healthcare). Purified Tα-S* was stored at -80 °C until use. Purity and the concentration of Tα-S* were assessed with SDS-PAGE, and the purity was almost 100 %. All of the manipulations for extraction and purification were performed at 4 °C.

Expression and purification of recombinant PDEγ

DNA sequence of frog PDEγ (GenBank Accession Number AB578858.1) was inserted into NdeI/BamHI sites of expression vector, pET-3a (Novagen). PDEγ was expressed in E. coli

BL21(DE3) pLysS strain (Novagen) after induction with IPTG for 3 hr at 30 °C. Purification of expressed PDEγ was carried out based on the method described previously (27, 28). Briefly, the cells expressing PDEγ were collected and sonicated in a buffer (buffer D: 50 mM Tris-HCl, 20 mM NaCl, 5 mM EDTA, 1 mM DTT, pH7.5) supplemented with 1 mM phenylmethylsulfonyl fluoride, and then the suspension was centrifuged at 12,000 × g for 30 min. The supernatant containing PDEγ was loaded on a CM Sepharose Fast Flow column (GE Healthcare) equilibrated with buffer D. The bound proteins were eluted using a 20 - 400 mM NaCl gradient in buffer D. Additional purification of PDEγ was carried out using a C18 reverse-phase column (Nacalai Tesque) with a 0 - 42 % gradient of acetonitrile in 0.1 % (v/v) trifluoroacetic acid (TFA) dissolved in H_2O. Purified PDEγ was lyophilized to remove acetonitrile and TFA, and dissolved in K-gluc buffer and stored at -80 °C until use.

*Immobilization of Tα–S**

To immobilize Tα–S* on the sensor chip for the SPR measurement, Tα–S* was first biotinylated at its thiol groups. For this purpose, 3.3 µl of 2 mM EZ-Link Maleimide-PEG$_2$-Biotin (Thermo Fisher Scientific) was added to 100 µl of 13 µM of purified Tα-S* in K-gluc buffer without DTT, and the mixture was incubated for 1 hr on ice. After the incubation, 0.35 µl of 1 M DTT was added to reduce and deactivate the non-reacted maleimide group of Maleimide-PEG$_2$-Biotin. Then, the buffer was changed to K-gluc to remove the deactivated Maleimide-PEG$_2$-Biotin using a Zeba Spin Desalting Column (Thermo Fisher Scientific).

Purified biotinylated Tα-S* was immobilized on a streptavidin (SA) sensor chip (GE Healthcare) through the streptavidin-biotin interaction. There are 8 thiol groups in Tα-S* (NCB Accession # NM_181022.2). However, my analysis revealed that PDEγ bound only to Tα-S*

that allows high affinity binding of PDEγ.

Measurement of the bindings of PDEγ and PDE to Tα-S* with SPR, and its analysis

The binding of PDEγ and that of PDE to Tα-S* were measured using Biacore X100 (GE Healthcare). The common binding target, biotinylated Tα-S* was immobilized in flow cell 2 which is connected to flow cell 1, a reference cell, in tandem. Immobilization level was mostly <400 resonance unit (RU), but in the measurement shown in Fig. 1, it was ~2300 RU. In flow cell 1, an SA sensor chip was treated with Maleimide-PEG$_2$-Biotin of which maleimide had been deactivated by DTT.

A solution containing purified recombinant PDEγ or purified PDE sample was injected at various concentrations for desired time periods, and the bound molecules were washed out each time with a running buffer (K-gluc buffer containing 0.005 % (v/v) Tween 20). All these experiments were performed at 25 °C and at a flow rate of 10 μl/min. Binding signals of PDEγ or PDE, essentially the signals obtained in flow cell 2 minus those in flow cell 1, were processed with the SPR instrument used. I used two ways to record the binding, one with binding and dissociation both terminated before their completion (Figs. 4 and 7b) and the other after their completion (Fig. 7a).

When necessary, the binding data were analyzed by BIAevaluation software (GE Healthcare) to determine K_{D2}. The programs used are designed to include one of the crucial effects, mass transport effect (MTL) (29). For the analysis of binding signals of PDEγ to immobilized Tα-S*, I used Heterogeneous Ligand with MTL program with assuming that there are at least two populations of Tα-S* immobilized differently depending on which thiol site was immobilized. However, my analysis indicated that the binding of PDEγ to immobilized Tα-S* consisted of only one major component (>98 %).

Measurement of the binding of Tα-S* to immobilized PDEγ with SPR (reversed configuration)

Recombinant PDEγ was immobilized at its lysine amino groups on a carboxymethylated dextran (CM5) sensor chip (GE Healthcare) in flow cell 2 using 1-ethyl-3-(3-dimethylaminopropyl)-carbodiimide (EDC) and N-hydroxysuccinimide (NHS) according to the manufacturer's protocol. NHS-ester formed but unreacted to PDEγ was blocked with ethanolamine after the immobilization. In the reference flow cell 1, CM5 sensor chip was treated similarly as in flow cell 2, but the formed NHS-ester was blocked directly with ethanolamine without exposure to PDEγ.

Tα-S* solutions of increasing concentrations were injected intermittently for 125 sec with washing out of the bound Tα-S* each time for 170 sec or more using a regeneration buffer ($\times$ 0.5 K-gluc buffer containing 0.0025 % of Tween 20 and 6 M of guanidine hydrochloride, pH7.5). Measurements were made at 25 °C and at a flow rate of 30 μl/min. Binding of Tα-S* to immobilized PDEγ was analyzed with a 1:1 Binding with MTL program.

There are 8 lysine residues in PDEγ (GenBank Accession Number X04270.1 in bovine and GenBank Accession Number AB578858.1 in frog; the amino acid sequences of PDEγ are the same in bovine and frog), and all of them (Lys-7 − Lys-45) are at the region outside of the major binding site of PDEγ to Tα-S* (Asp-63 - Ile-87 in PDEγ, ref. 5 and PDB # 2JU4). However, according to the crystal structure of PDEγ (PDB # 2JU4), four of them (Lys-25, Lys-29, Lys-31 and Lys-39) are near the Arg-33 and Arg-36 residues that have been reported to be involved in the binding of PDEγ to Tα* (30). Immobilization at one of these lysine residues would reduce the binding of Tα-S* to PDEγ because of steric hindrance. It would be the reason why I obtained a higher K_D in the reversed configuration (Fig. 7b) than that I observed in the binding of PDEγ to immobilized Tα-S* (Fig. 7a).

Determination of the K_{DI} of the PDEγ·PDEcat complex with dilution

PDE activity was measured using purified PDE at various concentrations of PDE (≤40 nM), both in the light without GTP. The activity was measured with the pH assay method using a combination glass microelectrode (MI-410, Microelectrodes, Inc.) as described previously (14, 16, 31). At time 0, 5 mM cGMP was added to initiate the hydrolysis. All measurements were performed at room temperature. To measure the full PDE activity, PDEγ was digested with trypsin (final concentration, 0.1 mg/ml) for 5 min at room temperature, and the digestion was terminated by adding trypsin inhibitor at a final concentration of 0.5 mg/ml. Then, the full PDE activity measurement was initiated with adding 5 mM cGMP.

PDE activation with Tα-S of various concentrations*

PDE activities at various concentrations of Tα-S* were measured with the pH assay method in a solution and in a ROS membrane suspension.　In　a　solution,　Tα-S*　of　known concentration was added to 15 nM purified PDE in K-gluc buffer in the light. At time 0, 5 mM cGMP (final concentration) was added to initiate cGMP hydrolysis. In a ROS membrane suspension, first 5 mM cGMP was added to purified ROS membranes containing 1.5, 10 or 20 μM rhodopsin in the dark, and the membranes were illuminated to activate rhodopsin fully. Then, GTPγS of known concentration was added to the membranes to initiate the cGMP hydrolysis. In the measurement in ROS membrane suspensions, concentrations of GTPγS were set so as to limit the amount of Tα-S* by the amount of GTPγS added (14). To estimate the concentration of transducin at different concentrations of ROS membranes, I assumed that molar ratio of transducin to rhodopsin is 1/10 (for example, 2 μM transducin present in 20 μM rhodopsin membranes). In both types of preparations, solution and membrane suspension, full PDE activity

34

was measured after trypsin digestion as described previously (14) to determine the relative PDE

activity (% max).

Formulation of dissociation of PDEγ from PDEcat

It is expected that PDEγ is freed from PDEγ·PDEcat complex depending on its K_D.

The reaction scheme is:

$$PDEγ + PDEcat \xrightleftharpoons{K_{D1}} PDEγ·PDEcat \qquad \text{- - - (Reaction 1),}$$

where K_{D1} is the dissociation constant of the PDEγ·PDEcat complex:

$$K_{D1} = [PDEγ]\,[PDEcat] / [PDEγ·PDEcat] \qquad \text{- - - (Equation 1).}$$

Because one PDE molecule is initially composed of two catalytic subunits and two PDEγ, the

following relation holds:

$$[PDEcat]total = [PDEγ] + [PDEγ·PDEcat]$$
$$= 2\,[PDE]total \qquad \text{- - - (Equation 2),}$$

where [PDEcat]total is the total concentration of the catalytic subunit, and [PDE]total is the total

concentration of PDE. In addition, [PDEcat] should be equal to that of freed PDEγ ([PDEγ]):

$$[PDEcat] = [PDEγ] \qquad \text{- - - (Equation 3)}$$

From Equations 1 – 3, I obtained a solution for [PDEcat]:

$$[\text{PDEcat}] = \left(-K_{D1} + \sqrt{K_{D1}^2 + 8K_{D1}[\text{PDE}]\text{total}} \right) / 2 \qquad \text{- - - (Equation 4).}$$

In Fig. 5, I expressed each PDE activity as the relative value to the full PDE activity measured in ROS membranes treated with trypsin (see Experimental Procedures). Relative PDE activity is obtained by dividing Equation 4 with [PDEcat]total, namely, 2[PDE]total (Equation 2):

$$\text{Relative PDE activity} = \left(-K_{D1} + \sqrt{K_{D1}^2 + 8K_{D1}[\text{PDE}]\text{total}} \right) / 4[\text{PDE}]\text{total} \quad \text{- - - (Equation 5).}$$

*Formulation of activation of PDE with Tα**

In the trapping mechanism, the reaction schemes can be written as follows.

$$\text{PDE}\gamma + \text{PDEcat} \quad \xrightleftharpoons{K_{D1}} \quad \text{PDE}\gamma\cdot\text{PDEcat} \qquad \text{- - - (Reaction 1),}$$

$$\text{PDE}\gamma + \text{T}\alpha^* \quad \xrightleftharpoons{K_{D2}} \quad \text{PDE}\gamma\cdot\text{T}\alpha^* \qquad \text{- - - (Reaction 2),}$$

where K_{D1} is the constant defined in the above and K_{D2} is the dissociation constant of the PDEγ·Tα* complex:

$$K_{D1} = [\text{PDE}\gamma]\,[\text{PDEcat}] / [\text{PDE}\gamma\cdot\text{PDEcat}] \qquad \text{- - - (Equation 1)}$$

$$K_{D2} = [\text{PDE}\gamma]\,[\text{T}\alpha^*] / [\text{PDE}\gamma\cdot\text{T}\alpha^*] \qquad \text{- - - (Equation 6).}$$

Total concentrations of PDEcat ([PDEcat]total), Tα* ([Tα*]total) and PDEγ ([PDEγ]total) are expressed as follows.

[PDEcat]total = [PDEγ·PDEcat] + [PDEcat] = 2[PDE]total   - - - (Equation 7)

[Tα*]total = [Tα*·PDEγ] + [Tα*]   - - - (Equation 8)

[PDEγ]total = [PDEγ] + [PDEγ·PDEcat] + [Tα*·PDEγ]

         = 2[PDE]total   - - - (Equation 9)

Using these relations, a cubic equation of [PDEcat] is obtained:

$(K_{D1} - K_{D2})$[PDEcat]^3

$+ (K_{D1}{}^2 - K_{D1} K_{D2} - 2 K_{D1}$ [PDEcat]total $+ K_{D1}$ [PDEγ]total $- K_{D1}$ [Tα*]total

$+ K_{D2}$[PDEcat]total $- K_{D2}$ [PDEγ]total)[PDEcat]^2

$- K_{D1}$ [PDEcat]total$(2 K_{D1} - K_{D2} -$ [PDEcat]total $+$ [PDEγ]total $-$ [Tα*]total)[PDEcat]

$+ (K_{D1}$ [PDEcat]total)^2

$= 0$ - - - (Equation 10)

The constants, K_{D1} and K_{D2}, are determined experimentally (Fig. 5 and Fig. 7, respectively), and [PDEcat]total (2[PDE]total), [Tα*]total, [PDEγ]total (2[PDE]total) are all known in a measurement of PDE activity in Fig. 7 and Fig. 8. Then, Equation 10 can be solved to calculate [PDEcat] numerically at a given Tα* (actually Tα-S* in Fig. 8 and Fig. 9) concentration. PDE activity biochemically measured is expressed as the % of the full activity, and the dark activity is subtracted. To compare the biochemical and the theoretical result, [PDEcat] calculated at a given

[Tα*] in Equation 10 was divided by [PDEcat]total.

REFERENCES

1. Kawamura, S. & Tachibanaki, S. Rod and cone photoreceptors: Molecular basis of the difference in their physiology. *Comp. Biochem. Physiol. A Mol. Integr. Physiol.* **150**, 369–377 (2008).

2. Fu, Y. & Yau, K. W. Phototransduction in mouse rods and cones. *Pflugers Arch.* **454**, 805–819 (2007).

3. Leskov, I. B., Klenchin, V. A., Handy, J. W., Whitlock, G. G., Govardovskii, V. I., Bownds, M. D., Lamb, T. D., Pugh, E. N. Jr. & Arshavsky, V. Y. The Gain of Rod Phototransduction: Reconciliation of Biochemical and Electrophysiological Measurements. *Neuron* **27**, 525–537 (2000)

4. Dumke, C. L., Arshavsky, V. Y., Calvert, P. D., Bownds, M. D. & Pugh, E. N., Jr. Rod outer segment structure influences the apparent kinetic parameters of cyclic GMP phosphodiesterase. *J. Gen. Physiol.* **103**, 1071–1098 (1994)

5. Yamazaki, A., Stein, P. J., Chernoff, N. & Bitensky, M. W. Activation mechanism of rod outer segment cyclic GMP phosphodiesterase. Release of inhibitor by the GTP/GTP-binding protein. *J. Biol. Chem.* **258**, 8188-8194 (1983).

6. Wensel, T. G. & Stryer, L. Reciprocal control of retinal rod cyclic GMP phosphodiesterase by its γ subunit and transducin. *Proteins* **1**, 90–99 (1986).

7. Slep, K. C., Kercher, M. A., He, W., Cowan, C. W., Wensel, T. G. & Sigler, P. B. Structural determinants for regulation of phosphodiesterase by a G protein at 2.0 angstrom. *Nature* **409**, 1071–1077 (2001).

8. Guo, L. W., Muradov, H., Hajipour, A. R., Sievert, M. K., Artemyev, N. O. & Ruoho, A. E. The inhibitory γ subunit of the rod cGMP phosphodiesterase binds the catalytic subunits in an extended linear structure. *J. Biol. Chem.* **281**, 15412–15422 (2006).

9. Bennett, N. & Clerc, A. Activation of cGMP phosphodiesterase in retinal rods: Mechanism of interaction with the GTP-binding protein (transducin). *Biochemistry* **28**, 7418–7424 (1989).

10. Otto-Bruc, A., Antonny, B., Vuong, T. M., Chardin, P. & Chabre, M. Interaction between the retinal cyclic GMP phosphodiesterase inhibitor and transducin. Kinetics and affinity studies. *Biochemistry* **32**, 8636–45 (1993).

11. Slepak, V. Z., Artemyev, N. O., Zhu, Y., Dumke, C. L., Sabacan, L., Sondek, J., Hamm, H. E., Bownds, M. D. & Arshavsky, V. Y. An effector site that stimulates G-protein GTPase in photoreceptors. *J. Biol. Chem*. **270**, 14319–14324 (1995).

12. Wieland, T., Chen, C. K. & Simon, M. I. The retinal specific protein RGS-r competes with the γ subunit of cGMP phosphodiesterase for the subunit of transducin and facilitates signal termination. *J. Biol. Chem*. **272**, 8853–8856 (1997).

13. Pugh, E. N. & Lamb, T. D. Amplification and kinetics of the activation steps in phototransduction. *Biochim. Biophys. Acta.* **1141**, 111–149 (1993).

14. Koshitani, Y., Tachibanaki, S. & Kawamura, S. Quantitative aspects of cGMP phosphodiesterase activation in carp rods and cones. *J. Biol. Chem*. **289**, 2651–2657 (2014).

15. Arshavsky, V. Y., Dumke, C. L. & Bownds, M. D. Noncatalytic cGMP-binding sites of amphibian rod cGMP phosphodiesterase control interaction with its inhibitory gamma-subunits. A putative regulatory mechanism of the rod photoresponse. *J. Biol. Chem.* **267**, 24501-24507 (1992).

16. Yee, R. & Liebman, P. A. Light-activated Phosphodiesterase of the Rod Outer Segment. *J. Biol. Chem.* **253**, 8902-8909 (1978).

17. Kokame. K., Fukada, Y., Yoshizawa, T., Takao, T. & Shimonishi, Y. Lipid modification at the N terminus of photoreceptor G-protein alpha-subunit. *Nature* **359**, 749-752 (1992).

18. Barren, B., Gakhar, L., Muradov, H., Boyd, K. K., Ramaswamy, S. & Artemyev, N., O.

Structural basis of phosphodiesterase 6 inhibition by the C-terminal region of the gamma-subunit. *EMBO J.* **28**, 3613–3622 (2009).

19. Qureshi B. M., Behrmann, E., Schöneberg, J., Loerke, J., Bürger, J., Mielke, T., Giesebrecht, J., Noé, F., Lamb, T. D., Hofmann, K. P., Spahn, C. M. T. & Heck, M. It takes two transducins to activate the cGMP-phosphodiesterase 6 in retinal rods. *Open Biol.*, **8**, 180075 (2018).

20. Yamazaki, A., Tatsumi, M. & Bitensky, M. W. Purification of rod outer segment GTP-binding protein subunits and cGMP phosphodiesterase by single-step column chromatography. *Methods Enzymol.* **159**, 702–710 (1988)

21. Kühn, H. Light-regulated binding of proteins to photoreceptor membranes and its use for the purification of several rod cell proteins. *Methods Enzymol.* **81,** 556–564 (1982).

22. Kawamura, S. & Murakami, M. Regulation of cGMP levels by guanylate cyclase in truncated frog rod outer segments. *J. Gen. Physiol.* **94**, 649-668 (1986).

23. Baylor, D. A., Matthews, G., Yau. K. -W. Two components of electrical dark noise in toad retinal rod outer segments. *J. Physiol* **309**, 591-621 (1980).

24. Rieke. F. & Baylor. D. A. Molecular origin of continuous dark noise in rod photoreceptors. *Biophys. J.* **71**, 2553-2572 (1996).

25. Yau, K. -W. Phototransduction mechanism in retinal rods and cones. The Friedenwald Lecture. *Invest. Ophthalmol. Vis. Sci.* **35**, 9-32 (1994).

26. Papermaster, D. S. Preparation of Retinal Rod Outer Segments. *Methods Enzymol.* **81**, 48-52. (1982)

27. Wensel, T. G. & Stryer, L. Activation mechanism of retinal rod cyclic GMP phosphodiesterase probed by fluorescein-labeled inhibitory subunit. *Biochemistry* **29**, 2155–2161 (1990)

28. Guo, L. W., Hjipour, A. R., Gavala, M. L., Arbabian, M., Martemyanov, K. A., Arshavsky, V.

Y. & Ruoho, A. E. Sulfhydryl-reactive, cleavable, and radioiodinatable benzophenone photoprobes for study of protein-protein interaction. *Bioconjug. Chem.* **16**, 685–693 (2005)

29. Schuck, P. & Zhao, H. The role of mass transport limitation and surface heterogeneity in the biophysical characterization of macromolecular binding processes by SPR biosensing. *Methods Mol. Biol.* **627**, 15–54 (2010)

30. Bondarenko, V. A., Desai, M., Dua, S., Yamazaki, M., Amin, R. H., Yousif, K. K., Kinumi, T., Ohashi, M., Komori, N., Matsumoto, H., Jackson, K. W., Hayashi, F., Usukura, J., Lipkin, V. M. & Yamazaki, A. Residues within the polycationic region of cGMP phosphodiesterase γ subunit crucial for the interaction with transducin α subunit. Identification by endogenous ADP-ribosylation and site-directed mutagenesis. *J. Biol. Chem.* **272**, 15856-15864 (1977).

31. Tachibanaki, S., Shimauchi-Matsukawa, Y., Arinobu, D. & Kawamura, S. Molecular mechanisms characterizing cone photoresponses. *Photochem. Photobiol.* **83**, 19–26 (2007)

Acknowledgment

TABLES

Table 1. Fitted results of K_{D2} for purified PDE activation by Tα-S* in solution.

K_{D1} (constant, pM)	K_{D2} (fitted, nM)	χ^2
2.0	1.8	0.000546
3.0	2.7	0.000576
4.0	3.6	0.000611
5.0	4.5	0.000648
6.0	5.5	0.000688
7.0	6.4	0.000729
8.0	7.3	0.000772

Table 2. Fitted results of K_{D2} for PDE activation by Tα-S* in ROS membrane suspension.

[Rhodopsin] (μM)	K_{D1} (constant, pM)	K_{D2} (fitted, nM)	χ^2
	40.0	15.9	0.00425
	45.0	18.3	0.00466
1.5 μM	50.0	20. 9	0.00508
	55.0	23.6	0.00551
	60.0	26.4	0.00595
	40.0	0.147	0.000786
	45.0	0.164	0.000844
10 μM	50.0	0.182	0.000845
	55.0	0.201	0.000845
	60.0	0.219	0.000846
	40.0	0.0410	0.0332
	45.0	0.0462	0.0332
20 μM	50.0	0.0513	0.0332
	55.0	0.0565	0.0332
	60.0	0.0617	0.0332

Achievements

Publications

Peer-Reviewed Original Research Articles

1. <u>T. Asano</u>, S. Tachibanaki, S. Kawamura. Transducin activates cGMP phosphodiesterase by trapping inhibitory γ subunit freed reversibly from the catalytic subunit in solution. Sci. Rep. 投稿中

Conference Presentations

Oral:

1. <u>淺野禎三</u>・橘木修志・河村悟．表面プラズモン共鳴法によるコイ cGMP ホスホジエステラーゼ活性化反応の解析．第 86 回　日本動物学会　2015 年 9 月（新潟）

Poster:

1. <u>T. Asano</u>, S. Tachibanaki, S. Kawamura. Transducin activates cGMP phosphodiesterase indirectly. 54th Biophysical Society of Japan　Nov. 2016（Tsukuba）

2. 橘木修志・<u>淺野禎三</u>・河村悟．コイ桿体視細胞におけるホスホジエステラーゼ活性化機構の解析．第 88 回　日本動物学会　2017 年 9 月（富山）

3. 橘木修志・<u>淺野禎三</u>・河村悟. 桿体視細胞ホスホジエステラーゼ活性化機構は乖離安定化モデルで説明できるか？　第 89 回　日本動物学会　2018 年 9 月（札幌）